Available online at www.sciencedirect.com
SCIENCE DIRECT®
Journal of Magnetic Resonance 175 (2005) 256–263
JMR Journal of Magnetic Resonance
www.elsevier.com/locate/jmr

Plate form three-dimensional gradient coils for L-band ESR imaging experiment ☆

Wu Ke [a,b], Huang Changgang [c], Cong Jianbo [a], Xian Hong [a], Wang Changzhen [a], Gao Shangkai [b,*]

[a] Beijing Institute of Radiation Medicine, Beijing 100850, China
[b] Department of Biomedical Engineering, Medical School of Tsinghua University, Beijing 100084, China
[c] Institute of Electrical Engineering, Chinese Academy of Sciences, Beijing 100080, China

Received 7 February 2005; revised 12 April 2005
Available online 1 June 2005

Abstract

A set of plate form three-dimensional magnetic gradient coils was developed and used in electron spin resonance imaging (ESRI) experiment. The coils were processed with whole copper plates instead of wound with copper wires, which made its structure so compact that it was much thinner and smaller comparing to those traditionally used in ESRI. The coil set had a pie-like appearance of which the total thickness was only 14 mm and the outer diameter was 250 mm. The efficiency of the coils could be greater than 10 mT/m/A when distance between the two side-pieces was 63 mm. A maximum gradient strength of more than 200 mT/m could be obtained with driving current of about 20 A in each dimension coil. The spatial linearity was better than 5% in all three dimensions within the available spatial linearity area of larger than a sphere of 40 mm in diameter. The stability of the gradients strength could reach the level of 10^{-5}. An imaging resolution of better than 1 mm could be achieved with the coil set. Some preliminary practical imaging results show that the developed gradient coil set is suitable for L-band ESRI experiment of biological samples or even in vivo small animals.

Keywords: Gradient coil; Plate form; Three-dimension; ESRI

1. Introduction

Electron spin resonance imaging (ESRI) technique has been increasingly used in studies of determining the distribution or metabolism of some exogenous biologically active free radicals such as the nitroxide free radicals in biological systems [1–7]. Most ESRI apparatus used for biological research nowadays work in continuous wave L-band or lower frequency [8–11]. Therefore, a static gradient field is used. In biological ESR imaging, the volume of detected sample is usually larger than that used in normal ESR experiments. On the other hand, most ESR spectra are wider than those of nuclear magnetic resonance (NMR). So, in order to achieve good resolution images, the gradient magnetic field should be established with such properties that it should be able to provide a wide available gradient area and it should also be stable, high efficient as well as with relatively much stronger gradient strength and with good linearity.

Conventional gradient coils in use now are made of copper wires wound either in shape of "8" for gradient directions vertical to the main magnet or in reverse linked Helmholtz coils for gradient direction parallel to the main magnet [12]. Besides the complexity of its winding process, this kind of coils often have relatively

☆ Supported by the National Science Funds of China (Grant No. 29935080).
* Corresponding author.
E-mail address: gsk-dea@mail.tsinghua.edu.cn (G. Shangkai).

1090-7807/$ - see front matter © 2005 Elsevier Inc. All rights reserved.
doi:10.1016/j.jmr.2005.04.013

large volume that requires wider main magnet pole gap, which furthermore results in larger main magnet frame and lower efficiency of the whole magnet system.

In this study, a set of innovative three-dimensional gradient coils named plate form gradient coils was developed and first used for ESRI experiment. The newly developed coils were made out of whole copper plates by means of electric line cutting technique instead of wound with copper wires. Using this gradient coil set, a linear three-dimensional gradient field was established with good performance properties on a homemade L-band ESRI system developed in our laboratory. The comprehensive characteristics of the coil set and some preliminary ESRI application results show that the coil set is suitable for ESRI experiment in biomedical research work.

2. Materials and methods

2.1. Principle structure of the coils

The newly developed coil set includes two side-pieces that are fixed on the main magnet poles to produce gradient field between them. Each side-piece consists of three-dimension coil-pieces assembled together closely. The major design process of the coil includes two steps. First, the magnetic field at each prescribed point in the region of interest was calculated according to the Biot–Savart law. In this process, different working conditions have to be considered. For example, in our work, the two main magnet poles are located to outside of the coils, the poles were made of ferromagnetic materials. This is different from those superconducting MRI that works in air environment. The second step is the optimization of the coil shape. In this process, non-linearity was chosen as objective function and all geometry parameters that decide the coil shape were chosen as optimizing variables. The variable metathesis method was used in our optimization. Basically, the whole design process is similar in both principle and process with that introduced by Lu et al. [13]. The theoretical structures of the coil-pieces are shown in Fig. 1. If Z-dimension is defined to have the same direction with the main magnet, the structure of Z coil will be like that shown in Fig. 1A. In practice, coils need to work in pairs. In this work, the Z-dimension coil pair was similar to but not exact a pair of reversely linked *Helmholtz* coils. So, its properties such as linear area, gradient strength, homogeneity, etc., were also similar to those of reversely linked *Helmholtz* coils. Different from Z coil, the X and Y coils had the same structure as shown in Fig. 1B. The X- and Y-dimension gradient could be separately established just by assembling the two dimension coil-pieces in a way that they are both concentric and orthogonal to each other. They were much different from those conventional ones in that in the center area of the coil, the remained conductors composed a group of parallel wires that were homogeneously arranged and extend to a wide area in the coil center. Through these parallel conductors, a relatively wider gradient area with high homogeneity could be guaranteed. When electric currents flowing in the different half part of the coil-piece were reversed, a linear gradient field could be established in the center area between the two side-pieces. Eddy current loss may become one of the most important effects affecting the gradient linearity. The wide cross-section area of the conductors in the center part of the coil-piece may cause relatively serious eddy current loss. But because our ESRI system, like the most in using ones, also works with static gradients instead of pulse ones, the eddy current loss can be neglected in this work.

2.2. Coil processing and assembling

Pure copper plates of 3 mm in thickness were used for coil processing in this work. Each coil-piece was processed with a whole copper plate. The processing sketches of designed coils were first drawn on the copper plates. Then each coil was processed out of the copper plate according to the processing lines automatically by electric line cutting machine. Considering both the insulating property between coil turns and the efficiency of the coils, the width of cutting lines was controlled within 0.4 mm and the width of remained conductor was less

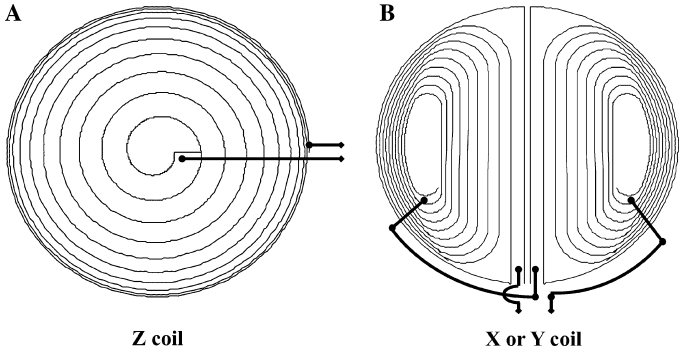

Fig. 1. Principle sketches of the coils. Thick lines indicate the connecting conductors to the power supplies.

than 4 mm. Finally, 38 turns for Z coil and 32 turns for X and Y coils were achieved in each coil-piece. The coil-pieces processed with this method had appearance of thin plate shape and could be well ensured to maintain symmetry in geometry. The connecting conductors of the coils were then led out in a way as that shown by the thick lines in Fig. 1. They were fixed at an appropriate position of the side-piece (shown in Fig. 3) for later connection to the output of driving power supplies.

The thin shape and compact structure of the coils made it easy to assemble the three-dimensional coil-pieces into one side-piece by sticking them together according to the principle construction of X-, Y-, and Z-dimension coil pairs as shown in Fig. 2. A saturation epoxy resin adhesive with strong adhering and good insulation property was used to stick the coil-pieces. To guarantee the insulation strength between coils, a piece of electrical insulating cloth was inserted between coil-pieces before sticking.

2.3. Driving power supplies

To simplifying the gradient control procedure of the gradient field as well as to get a stable gradient field, three sets of high precise constant current driving power supplies were developed with which the X-, Y-, and Z-dimension coils were individually driven. The stability of the gradient strength was mainly depended on that of the corresponding driving power supplies. Each dimension power supply could provide static current up to ± 22 A with current fluctuation of less than 0.01%. This current was strong enough to drive the respective coil pairs to generate gradient of up to 200 mT/m in either positive or negative direction according to the control signals. Gradient strengths were controlled by computer through three channels of 8-bit digital analog conversion port. The controlling precise was smaller than 1 mT/m (1/256 of 200 mT/m). In most biological imaging experiments, gradient often changes with an angle increment of 10° and the minimum change of gradient strength corresponding to such angle increment will be about 10 mT/m in any of an orthogonal axis. 1 mT/m is only 1/10 of the actual gradient changing. So, it is sufficient for gradient control of the most application cases. Even if smaller angle is used, such as 5°, it will bring about 1 mT/m minimum gradient strength change in the orthogonal axis. In this case, the 1 mT/m control precision is still workable.

3. Results and discussion

3.1. Basic characteristics of the coils

The appearance of the processed coil set is shown in Fig. 3. Its outer diameter is 250 mm, inner diameter 230 mm. The total thickness of all three-dimension coils is only 14 mm for one side-piece. The maximum number of turns is 32 turns for X and Y coil and 38 turns for Z coil. The impedances of the coils are 0.180, 0.182, and 0.184Ω, respectively for X, Y, and Z coils. As static current is used, inductive impedance of the coils is not considered.

3.2. Linearity

The spatial linearity of gradient field plays an important role in the resolution of reconstructed image. To determine the linearity of the gradient field set up with the developed coil set, constant static currents of 20.16, 19.68, and 18.11 A respective to X, Y, and Z coil were provided to generate the same gradient strength of 200 mT/m in each dimension. Magnetic strength was detected one point and another from the geometry center of the magnet field with increment step of 5 mm along each orthogonal axis. The detected area covered ± 20 mm from the center in each direction. A total num-

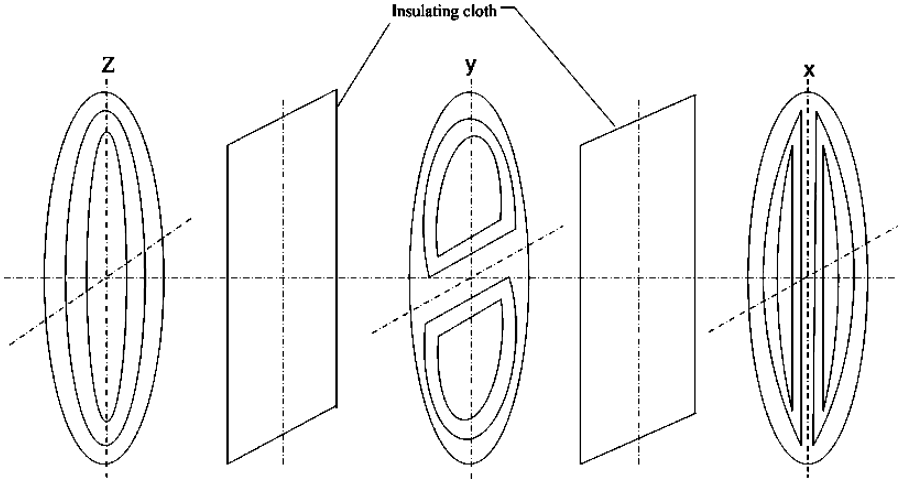

Fig. 2. Assembling method of the side-pieces.

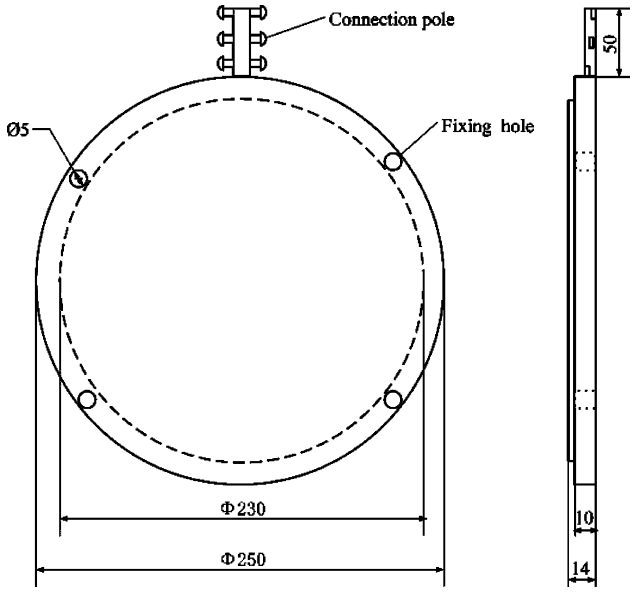

Fig. 3. Sketch of the assembled side-piece of the coil (scale: mm).

ber of 341 points were detected to complete the three-dimensions detection. According to the detected values, gradient strength along each dimension could be described as the following fitting equations that were obtained by the method of least squares:

X-dimension : $B_x = 200.36X - 0.02$;

Y-dimension : $B_y = 198.69Y - 0.50$;

Z-dimension : $B_z = 200.26Z - 0.58$.

The slope of each equation represents the mean gradient slope in respective direction. The calculated slopes from the detected values are not exact the fitting ones but a group of scat points distributing around the fitting values. According to this distribution, the spatial linearity of the gradient can be calculated by

$$\text{Linearity} = (\text{slope}_{\max} - \text{slope}_{\text{ave}})/\text{slope}_{\text{ave}} \times 100\%.$$

The $\text{slope}_{\text{ave}}$ is obtained from $(\text{slope}_{\max} + \text{slope}_{\min})/2$, the $\text{slope}_{\max}$ and $\text{slope}_{\min}$ represent the maximum and minimum gradient slope in specific direction. The ultimate linearity results were 4.43, 3.16, and 4.90%, respectively, to X-, Y-, and Z-dimension. Spatial linearity properties of the three-dimensions gradient are shown in Fig. 4. According to the detected values of the spatial linearity area introduced above, if we defined the inner tangent sphere of the detected cubic area as available effective working space of the three dimension gradient field, it would not be smaller than a sphere of 40 mm in diameter, which would be large enough for measurement of most kinds of biological samples like animal organs or even whole small animals.

Besides the slope, there is also a constant part in each fitting equation. The constant part should be zero theoretically if the volume of the Gauss meter probe used to detect the magnet strength was small enough to be set exactly at the correct geometry center of the detecting area. At present condition, the maximum effect on the gradient induced from this reason was less than 0.3%. This effect was so trivial that it could be ignored comparing to those notable ones such as the non-linearity effect, etc.

As shown in Fig. 1, each coil has two short connecting conductors overlapping with the coil. Comparing to the whole coil, the contribution to the non-linearity from the connecting conductors would be very weak. This is demonstrated by the good gradient linearity as shown in Fig. 4.

The comparison of major technical features of the coils obtained from theoretical calculation and experiment were shown in the following table (Table 1).

Some differences can be seen between the data from design calculation and experiment. Most of the differences in linearity might be caused by the manufacturing

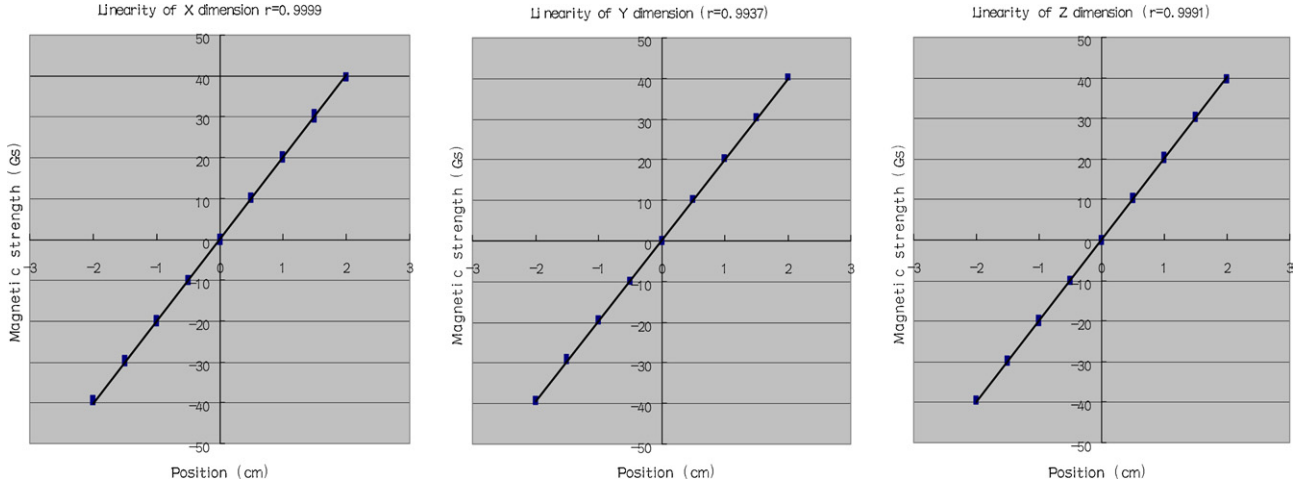

Fig. 4. Linearity of the gradient field.

Table 1
Some technical features of the coil set obtained from theoretical calculation and experiment

Items	Theoretical calculation	Experiment result
Region of interest (ROI)	Sphere region 42 mm in diameter	Cubic region $40 \times 40 \times 40$ mm^3
Maximum gradient strength	200 mT/m for all three dimensions	*X*: 200.4 mT/m *Y*: 198.7 mT/m *Z*: 200.3 mT/m
Linearity		
X	2.27%	4.43%
Y	1.39%	3.16%
Z	0.58%	4.90%
Resistance		
X	0.124 Ω	0.180 Ω
Y	0.124 Ω	0.182 Ω
Z	0.108 Ω	0.184 Ω

Table 2
Stabilities of the three-dimension driving power supplies

Dimension	*X*	*Y*	*Z*
Test time (h)	1	1	1
Max. current (A)	22.1303	22.3507	21.7291
Min. current (A)	22.1294	22.3489	21.7280
Stability	2.1×10^{-5}	4.2×10^{-5}	2.6×10^{-5}
Test meter	HP34401A		
Sensor	HITEC/100A, Model:ST-1, DC current transductor		

and detecting process. For the *X* and *Y* coils, a considerable non-linearity came from design process. The differences of the impedance between calculation and experiment might come from the resistors of connecting wires and resistors of the joining or attaching points in the circuit.

3.3. Stability of the gradient strength

As described above, the gradient fields were generated by constant current power supplies. The stability of the gradient mainly depended on the stability of the driving power supplies. Table 2 shows the stability of the driving power supplies in one hour duration. All the three power supplies had the stability level of 10^{-5}, which was good enough to perform ordinary ESRI experiment.

Another important factor relates to the stability of ESRI system is the temperature changing property of the coil set. As introduced above, in stead of being controlled by a *Hall* detector involved close-loop controlling system as those normally used in traditional ESRI apparatus, our gradient field was simply controlled by a group of constant current power supplies of which the output currents had been maintained constantly at precise of 10^{-5}, even if there was some fluctuation in their impedances caused by temperature rising of the coils or some other reasons. Therefore, the temperature changing of the coil set could hardly affect the stability of the gradient. Any way, a serious temperature fluctuation would still bring some disadvantage influences on the detected objects especially in some biological experiments when there was no water-cooling system in the coil set. From this point of view, temperature changing of the coils still became a considerable factor. The temperature changing effects of the coil set was detected in conditions of maximum working current and 65% of the maximum working current. The experiment was carried out at an environment temperature of 22 °C and with an electrical fan blowing 30 cm away from the coil set. The temperature readings were taken from an electrical thermo sensor stuck on the surface of the coil set. Fig. 5. shows the temperature changes of full and 65% of the working current conditions, respectively. The result of Fig. 5B indicates that the highest temperature can reach about 45 °C and it can be maintained below such level. Generally, conventional ESRI experiments work in the principle of *zeugmatography* [14]. Accordingly, the ultimate gradient strength is obtained

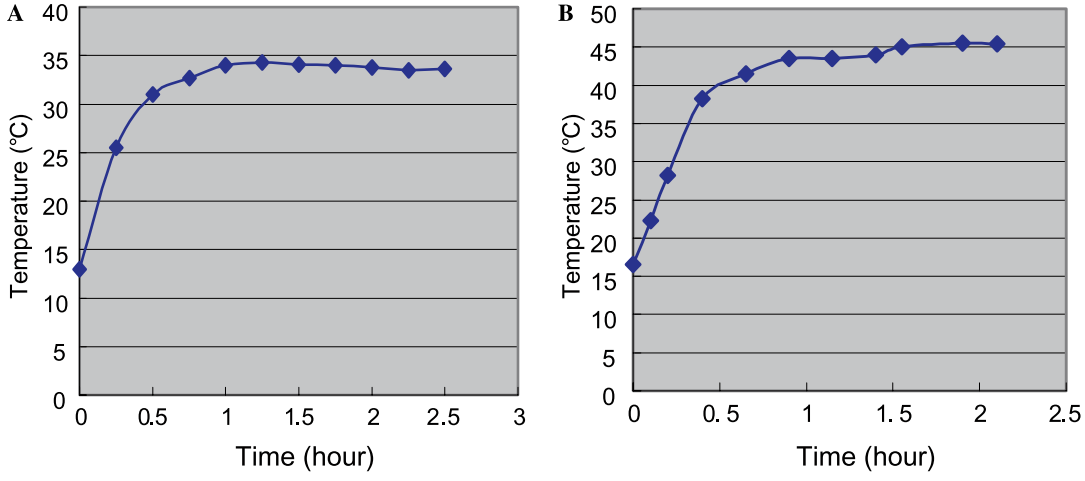

Fig. 5. Temperature variation of the coil set at room temperature (22 °C). (A) 65% load currents (20 A for *X* and 18 A for *Z* coil); (B) full load current (20 A for *X* and *Y* coil and 18 A for *Z* coil).

from the accumulation of the three orthogonal ones. Therefore, the gradient strength in each dimension is barely as high as that generated from full load current. It is only about $1/\sqrt{2}$ of the maximum one. In biological imaging, the normally used strength, such as often used for nitroxide free radical imaging, is only 60 mT/m. That is about 30% of the maximum strength. So, the temperature can not reach over 35 °C as displayed in Fig. 5A. That can hardly bring remarkable effects on ESRI experiments when there is an air gap between coil set and sample cavity to ensure an efficient air flowing.

3.4. Imaging resolution

The imaging resolution achieved by this gradient coil set was determined by two DPPH point samples of 1 mm in diameter. The two samples were separated less than 1 mm apart. The resolution experiment was carried out on this gradient coil set combining with a home-made L-band ESR system developed in our lab. Its main and scan magnet had homogeneity of 10^{-5}. The sample cavity was an re-entrance resonator similar to that described by Sotgiu [15]. Two-dimensional resolution was mainly considered because the extension to three-dimensional case was straightforward on the condition of the similar gradient linearity in all three dimensions as described above. A group of total 18 projection spectra were acquisitioned at gradient strength of 1.5 mT/cm with the gradient direction turning in an angle increment of 10°. Before image reconstruction, spectra were first processed as follows: noise filtering, baseline correcting, double integrating, and resolution enhancement by convolution difference technique. The processed spectra were then used as projections for the two-dimensional image reconstruction. To avoid some artifacts in the image, a filtering process to the image was carried out before plotting. In this process, the standard deviation of the image was subtracted from each element of the image. Then, a filtering process was carried out by the function of Wiener2 provided from the software of Matlab Version6.1. This filtering process method was determined by several pretests until the artifacts could not be seen on the image. Fig. 6 shows the samples' position, the typical projection spectra and the imaging result. The image clearly identifies the two samples. This means that the imaging resolution obtained with the developed gradient coil set can be better than 1 mm.

4. Applications

To verify the applicability of the coil set, some preliminary imaging experiments have been carried out with simple biological ESRI models. Fig. 7 shows the

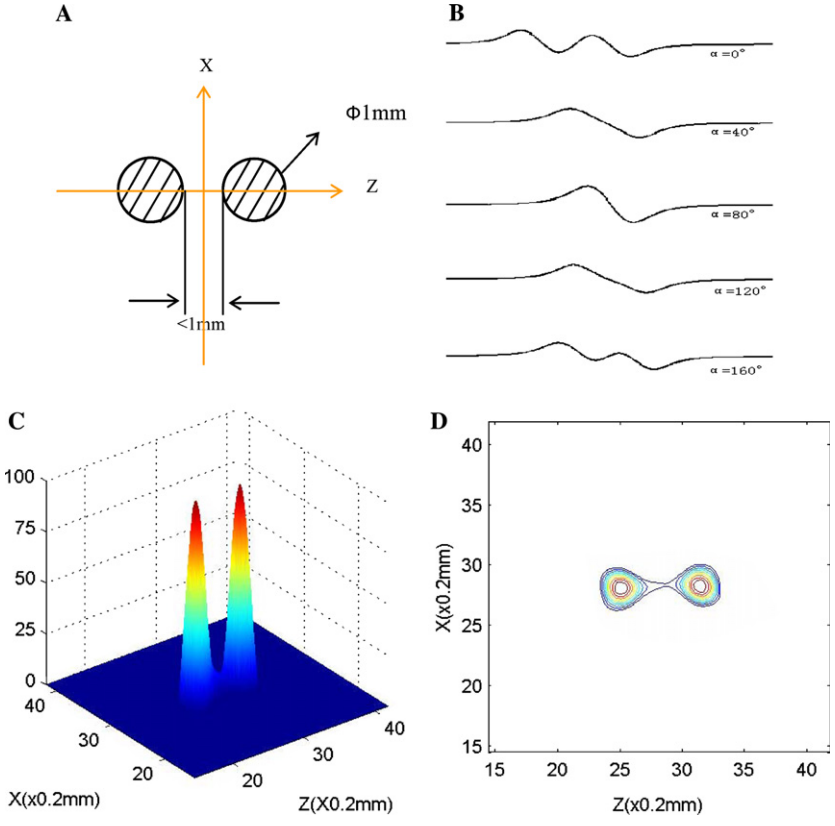

Fig. 6. Imaging resolution of 2D imaging experiment. (A) Sketch of the detected samples; (B) projections in different gradient angles; (C) image of the spin density; (D) contour image of the spin density.

Fig. 7. Two-dimensional ESR image of CTPO distributed in the body of mouse fetus.

imaging result of a mouse fetus. A normally used nitroxide free radical 3-carbamoyl-2,2,5,5-tetramethyl-3-pyrroline-1-yloxy (CTPO) was used as ESR signal donor. The mouse fetus was soaked in the CTPO solution with original concentration of 5×10^{-3} mol/L for 30 minus to make the nitroxide free radical compound penetrate through skin and some open organs, such as ears or anus and navel. In this way, the CTPO compound got an inhomogeneous dispersion in the animal's body. Field gradient strength of 60 mT/m was applied and its direction was changed from 0° to 180° with 20° increment steps. The acquisition scan rate was 10 s for each projection. The incident microwave power to the cavity was 80 mW. Time constant of the receiver was 0.2 s. Nine spectra were recorded for two-dimensional image. Similar process for image reconstruction and noise filtering was carried out as described above in this paper. The image clearly demonstrates the inhomogeneous distribution of CTPO solution in the body of the mouse fetus.

5. Conclusions

This work has first applied the plate form gradient coils that was specially designed and processed for L-band ESRI. The imaging results indicate the success of the attempt. Unlike conventional gradient coils, the newly developed coils are not wound with copper wires but made out of whole copper plates by means of electric line cutting technique. Therefore, the structure of the coils is so compact that it is much thinner and smaller than those traditionally used in ESRI. The compact structure made the coils convenient to be assembled on most kinds of ESR magnet frame, which results in a substantial decrease of the main magnet frame and furthermore lead to higher efficiency of the whole ESR magnet system. From the viewpoint of generating magnetic gradient, there are not great differences from the plate form coils to those made by other ways. But in some applying conditions, the thin shape of the plate coil set indeed has some advantages over others especially in conditions of narrow magnet gap.

Plate form coils have many advantages such as their compact structure, easy to process, high efficiency, good linearity, and low working noise, etc. But in some working conditions, they also have an inevitable intrinsic disadvantage. It is the eddy current loss caused by the relatively wide cross-section of the electric conductors in the central area of the coils. This effect will be fatal if the coils work in conditions of alternating current or even pulse current. Most current ESRI apparatus use static gradient field, thus the eddy current loss induced from the corresponding static current is puny and can be neglected.

The preliminary experiment results suggest that the newly developed plate form gradient coils are suitable for conventional ESRI experiment and will get more applications along with gradual improvements.

Acknowledgments

This work was supported by grants from the National Science Funds of China (No. 29935080). Thank Zheng Yingguang, Xu Jing, Dong Fengxia, Shen Erzhong, and Xu Yushu (from Jilin University) for helping with the ESR imaging apparatus, Cao Yuanlin and Xie Yuxiang (from Institute of Biophysics, Chinese Academy of Sciences) for providing with the mice fetus and helping with the animal imaging model in this work.

References

[1] L.J. Berliner, H. Fujii, X. Wang, et al., Feasibility study of imaging a living murine tumor by electron paramagnetic resonance, Magn. Reson. Med. 4 (1987) 380–384.
[2] J.L. Zweier, M. Chzhan, A. Samouilov, Electron paramagnetic resonance imaging of the rat heart, Phys. Med. Biol. 43 (7) (1998) 1823–1835.
[3] M. Velayutham, H.H. Li, P. Kuppusamy, J.L. Zweier, Mapping ischemic risk region and necrosis in the isolated heart using epr imaging, Magn. Reson. Med. 49 (2003) 1181–1187.
[4] H. Yokoyama, O. Itoh, M. Aoyama, H. Obara, H. Ohya, H. Kamada, ESR imaging for estimating oxidative stress in the brain of rats, Anal. Sci. 17 (2001) 1431–1432.
[5] M. Afeworki, G.M. Dam, N. Devasahayam, et al., Three-dimensional whole body imaging of spin probes in mice by time-domain radiofrequency electron paramagnetic resonance, Magn. Reson. Med. 43 (2000) 375–382.
[6] G.L. He, A. Samouilov, P. Kuppusamy, J.L. Zweier, In vivo imaging of free radicals: applications from mouse to man, Mol. Cell. Biochem. 234–235 (1–2) (2002) 359–367.
[7] M. Elas, B.B. Williams, A. Parasca, et al., Quantitative tumor oxymetric from 4D electron paramagnetic resonance imaging (EPRI): methodology and comparison with blood oxygen level-dependent (BOLD) MRI, Magn. Reson. Med. 49 (2003) 682–691.

[8] H. Yokoyama, H. Ohya, The recent in vivo ESR imaging in yamagata, Anal. Sci. 17 (2001) 511–514.
[9] V. Quaresima, M. Ferrari, Current status of electron spin resonance (ESR) for in vivo detection of free radicals, Phys. Med. Biol. 43 (7) (1998) 1937–1947.
[10] B.B. Williams, H. Hallaq, G.V.R. Chandramouli, et al., Imaging spin probe distribution in the tumor of a living mouse with 250 MHz EPR: correlation with BOLD MRI, Magn. Reson. Med. 47 (4) (2002) 634–638.
[11] D.J. Lurie, Free radical imaging, Br. J. Radiol. 74 (2001) 782–784.
[12] K. Ohno, ESR imaging and its applications, Appl. Spectrosc. Rev. 22 (1) (1986) 1–56.
[13] H. Lu, A. Jesmanowicz, S.J. Li, J.S. Hyde, Momentum-weighted conjugate descent algorithm for gradient coil optimization, Magn. Reson. Med. 51 (2004) 158–164.
[14] P.C. Lauterbur, Image formation by induced local interactions: examples employing nuclear magnetic resonance, Nature 242 (16) (1973) 190–191.
[15] A. Sotgiu, Resonator design for in vivo ESR spectroscopy, J. Magn. Reson. 65 (1985) 206–214.